Biointerface Research in Applied Chemistry
Open-Access Journal (ISSN: 2069-5837)

Article
Volume 13, Issue 2, 2023, 143
https://doi.org/10.33263/BRIAC132.143

Optical and Chemical Investigations of PEO Thin Films Incorporated with Curcumin Nanoparticle: Effect of Film Thickness

M-Ali AL-Akhras [1], Mahmoud Telfah [1], Musab N. Shakhatreh [1], Ahmad. Telfah [2], Marwan S. Mousa [3], Venkatesha Narayanaswamy [4], Ihab M. Obaidat [4,*]

[1] Bio-Medical Physics Laboratories, Department of Physical Sciences, Jordan University of Science & Technology, P.O. Box 3030, Irbid-22110, Jordan; alakmoh@just.edu.jo (M.A.A); telfah.mahmoud@googlemail.com (M.T); musab.shakhatreh1993@gmail.com (M.N.S).
[2] Leibniz-Institut für Analytische Wissenschaften - ISAS - e.V. 44139 Dortmund, Germany; telfah.ahmed@gmail.com (A.T).
[3] Department of Physics, Mutah University, Al-Karak 61710, Jordan; mmousa@mutah.edu.jo (M.S.M);
[4] Department of Physics, United Arab Emirates University, Al-Ain 15551, UAE; venkateshnrn@gmail.com (V.N); iobaidat@uaeu.ac.ae (I.M.O);
* Correspondence: iobaidat@uaeu.ac.ae (I.M.O.);

Scopus Author ID 10440642200
Received: 30.12.2021; Accepted: 26.01.2022; Published: 27.03.2022

Abstract: Using the spin coating technique, polyethylene oxide (PEO)-Curcumin nanocomposite thin films have been deposited on a quartz substrate. The film thickness role on the optical properties was investigated. SEM investigated the morphology of the thin films and revealed that curcumin NPs have a spherical shape with an average size of less than 100 nm. FTIR bands observed at 1023 and 1120 cm^{-1} correspond to C–O stretching vibration. New bands observed for the thin films at 804, 1237, 1280, and 1340 cm^{-1} correspond to C–H, C–O, and O-H bending. The thin films' optical properties with thickness 250, 500, and 750 nm were acquired from transmittance, reflectance, Tauc plot, extinction coefficient, and reflective index. The refractive index obtained from UV-Vis data falls between 1.5 and 2. Bandgap energy obtained for PEO thin film is 4.16 eV, while for both curcumin NPs and PEO-Curcumin nanocomposite thin films, the bandgap energy is 2.49 eV. Our results indicate that the optical absorption coefficient increases with decreasing film thickness. The obtained results are in good agreement with the existing reports.

Keywords: curcumin; PEO; spin coating; nanocomposite; optical properties; morphological properties.

1. Introduction

Curcumin is commonly used as an active ingredient in ancient herbal remedies, cosmetics, and food flavoring; it also promises a natural medicinal product in therapy [1–4]. It is often considered one of the most popular plants worldwide as an herbal medicinal product and reduction agent [5]. Curcumin (*Curcuma longa*) is a bright yellow chemical product found in a solid or powder form. Chemically, curcumin is a diarylheptanoid organic material that belongs to the category of curcuminoids that are natural phenols responsible for the gold color of turmeric. As a keto, it occurs as an enolic compound in organic solvents and water [6]. Curcumin is used to understand the light absorption behavior, with wide absorption band-

groups [7]. Laboratory and clinical research have noticed important medical treatment uses as anti-cancer such as skin, breast, liver, and colon cancer [6,8–10]. Curcumin's therapeutic potential is still debated despite its safety and efficacy due to poor water solubility and relatively poor bioavailability in humans, even when administrated at a high dosage of 12 g/da [11,12]. Medicinal chemistry has shown curcumin to be an unstable, reactive, non-bioavailable compound [13]. Many curcumin applications include flavoring foods and industrial products in southeast Asia [5]. Chemical structure of curcumin ($C_{18}H_{20}FN_3O_4$) enol form is 1E, 6E-1,7-Bis(4-hydroxy-3-methoxyphenyl) hepta-1,6-diene-3,5-dione. The molecular structure of curcumin is shown in Figure 1.

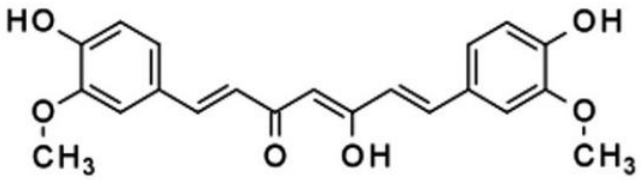

Figure 1. Curcumin ($C_{18}H_{20}FN_3O_4$-Enol form) molecular structure.

The curcumin structure ($C_{18}H_{20}FN_3O_4$) consists of aromatic phenolic rings threaded by two α, β-unsaturated carbonyl groups. Polyoxyethylene (PEO) has several industrial and biomedical applications. The molecular structure of the PEG is usually referred to as H−(O−CH_2−CH_2)n−OH [13]. PEO membranes are extensively studied for biomedical applications; PEO-nanoparticle membrane composite possesses improved properties over the individual components. PEO is used as a host polymer because of its high refractive index, absorption coefficients, and low bandgap energy compared to other hosts [9,14–16]. PEO is often used in clinical applications because of its physical properties, flexibility, ease of handling, processing, and low cost [13]. Polyethylene glycol and electrolytes are usually used for spontaneous bowel preparation before surgery or colonoscopy [17]. The chemical compound of polyethylene oxide (PEO) is shown in Figure 2. The study presented here mainly focuses on the optical and chemical properties of PEO-Curcumin nanocomposites. The role of film thickness on the optical properties is revealed.

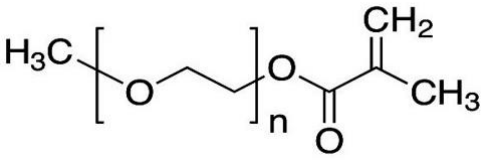

Figure 2. Molecular structure of polyethylene oxide (PEO).

2. Materials and Methods

PEO-curcumin nanocomposite thin films were prepared using the spin-casting technique. Additionally, a set of samples with different thicknesses 250, 500, and 700 nm were prepared. Oxygen plasma was used to clean and activate the quartz substrate surfaces.

2.1. Substrate activation.

The Quartz substrate was cleaned from the oxidization and adhesive layers before thin-film depositions of PEO-Curcumin to prevent contamination from the substrate. Then, distilled

water and ethanol were used to activate the substrates; the coated thin films were heated and dried in an oven at 30°C.

2.2. Preparation of PEO-Curcumin.

Curcumin NPs ($C_{18}H_{20}FN_3O_4$-Enol form-1E,6E-1,7-Bis(4-hydroxy-3-methoxyphenyl) hepta-1,6-diene-3,5-dione) were obtained from Sigma-Aldrich. Curcumin with a molar mass of 368.38 g/mol was used as received from Sigma-Aldrich. 0.5 g of PEO obtained from Sigma-Aldrich is dissolved in 500 mL of deionized water, then 100 mL of this solution is taken in a beaker along with 4.1 mg of curcumin nanoparticles. This solution dispersion is used as a stock solution for further thin-film fabrication. The mixture was heated and homogenized using an ultrasonic bath for more than 24 hours at 60°C. Suspended and large particles were excluded from the solution by centrifuging the solution repeatedly for 15 minutes per cycle. An ultra-fine ceramic filter was used to enhance the clarity of the solution. The mixture solution was heated and homogenized using an ultrasonic homogenizer at 25 °C for a few hours. The spin-casting technique used the PEO-Curcumin solution to prepare thin films with thicknesses 250, 500, and 750 nm.

3. Results and Discussion

3.1. SEM micrograph for curcumin NPs.

SEM images of the thin films were obtained under an operating voltage of 10 kV; the SEM micrographs are shown in Figure 3. The SEM images confirm the presence of curcumin NPs distributed over the membrane randomly. The curcumin particles are spherical, and the average particle sizes are less than 100 nm with significant size distribution. The curcumin NPs are arranged as clusters over the PEO films; this can be attributed to the low solubility of curcumin in the water medium.

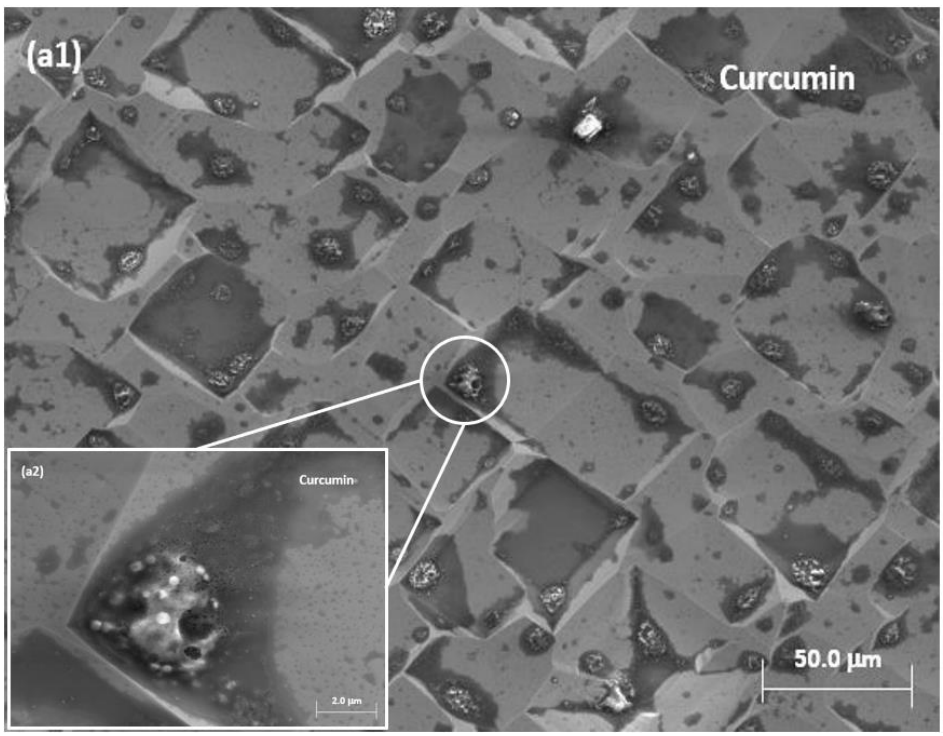

Figure 3. SEM micrograph of curcumin NPs.

3.2. FTIR spectroscopy.

Fourier Transform Infrared spectra of PEO and PEO-composite membranes are shown in Figure 4, representing the PEO-Curcumin nanoparticle composite's vibrational bands. The FTIR spectra consist of the characteristic peaks of both PEO and curcumin. The spectrum exhibits typical vibrational bands of PEO at 1023 and 1120 cm^{-1}, which correspond to the stretching of C–O bond, a peak at 1453 cm^{-1} corresponds to the $–CH_2$ bending vibration, the peak obtained in the 2950–2,700 cm^{-1} range is attributed to the symmetric and asymmetric stretching modes of the CH_2 group. PEO-Curcumin nanoparticles have additional peaks at 804, 1237, and 1280 cm^{-1}, which correspond to curcumin structure, i.e., vibrational bands at cm^{-1} that is assigned to bending of C–H, a band at 1237 and 1280 cm^{-1} that could be related to the C–O bending vibration and bands appearing in the 1340 cm^{-1} could be related to O-H bending. It is shown that there are significant changes observed in width and the intensity of the vibrational bands of PEO upon the formation of curcumin nanoparticle composite film. Such conformation shifts, referring to infrared active vibrational bands with ether oxygen, indicate alkali metal ions' complexation to ether oxygen [18–20].

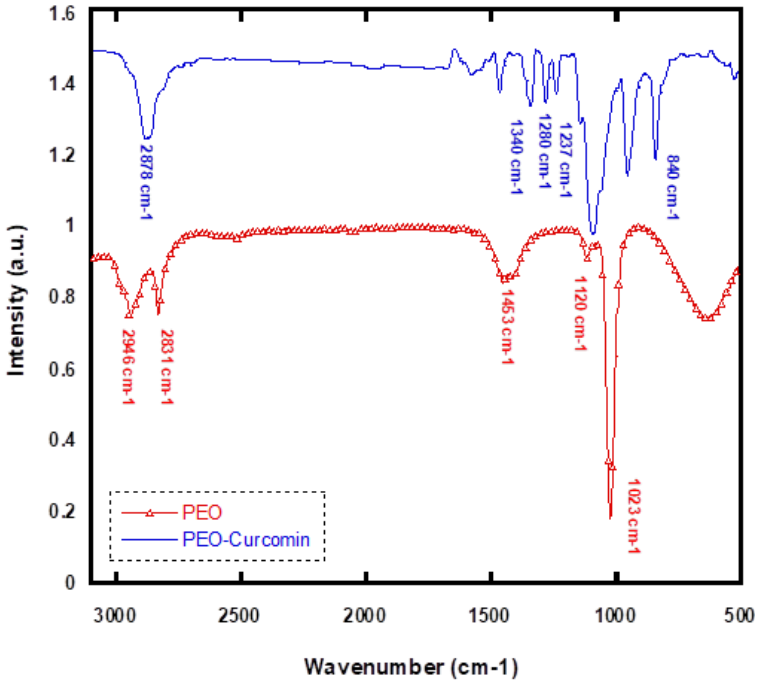

Figure 4. FTIR spectrum of PEO and PEO-Curcumin nanocomposite thin film.

3.3. UV-Vis spectroscopy.

UV-Visible spectra of PEO and PEO-Curcumin nanocomposite thin films were obtained in the range of 250-700 nm (T% and reflectance R% spectra). Transmittance and reflectance spectra were used to investigate all-optical properties to obtain the relevant parameters for optoelectronic applications. The UV-Visible transmittance spectra of PEO, curcumin, and PEO-Curcumin with an average thickness of 500 nm are shown in Figure 5. Comparable transmittance values were noticed between curcumin and PEO-Curcumin with cut-off below 600 nm, while PEO membrane has the transmittance cut-off start below 340 nm. This significant difference between these two cut-offs is due to the high absorption around the curcumin's maximum absorption peak.

Furthermore, it has been observed that PEO thin film exhibits high transmittance above 300 nm, while curcumin thin film exhibits high transmittance above 600 nm. PEO-Curcumin nanocomposite thin film also has high transmittance above 600 nm. This emphasizes that the bandgap energy for curcumin is less than PEO. The absorption region's edge was shifted into a red region with lower energy upon forming PEO-Curcumin nanocomposite thin film. This is attributed to the high electron transition from valence band and conduction band for curcumin using which band gap is obtained.

The reflectance spectra of PEO, curcumin, and PEO-Curcumin nanocomposite thin film with an average thickness of 500 nm are shown in Fig. 6. PEO thin films' reflectance values were found to be in the range of 11- 6% when the wavelength gradually decreased from 700 to 336 nm. On the other hand, the reflectance values of curcumin and PEO-Curcumin ranged from 15-3.5 % as the wavelength decreased rapidly from 800 to 560 nm, while the reflectance values sharply increased in the UV region from 360 to 250 nm. Thus, the reflectance values of PEO-Curcumin are significantly higher than PEO and curcumin, whereas the reflectance values are comparable for curcumin and PEO-Curcumin in the range of 336 – 530 nm.

Bandgap energy is obtained by the Tauc plot, which is the most acceptable method. It is defined by the absorption coefficient with the incident photon energy $\boldsymbol{h\nu}$ as $(\boldsymbol{\alpha h\nu})^{\boldsymbol{1/n}} = \boldsymbol{\beta}(\boldsymbol{h\nu} - \boldsymbol{E_g})$ [21,22], where: α is absorption coefficient, β is constant called band tailing parameter, E_g is the bandgap energy, were estimated from Tauc's plot by extrapolating a tangential line to hυ axis, and n is a factor of the power of the transition mode (for direct allowed transitions of PEO thin films, n = 0.5), which corresponds to the nature of the material [23]. Tauc plot has been used by plotting the incident energy of the photon ($\boldsymbol{h\nu}$) in eV against $(\boldsymbol{\alpha h\nu})^{\boldsymbol{2}}$. Figure 7 illustrates the Tauc plot for PEO, curcumin, and PEO-Curcumin samples, the linear part of incident photon energy was plotted to determine the bandgap energy. Bandgap energy ($\boldsymbol{E_g}$) is the intercept with the x-axis (incident photon energy). PEO thin film's bandgap energy was found to be 4.16 eV, while curcumin and PEO-Curcumin nanocomposite thin film has a bandgap energy of about 2.49 eV.

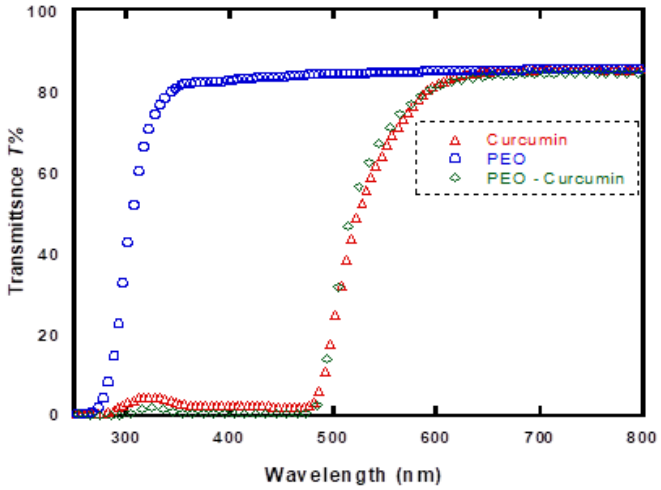

Figure 5. Transmittance spectra of PEO, curcumin, and PEO-Curcumin thin films with an average thickness of 500 nm.

These results could be significantly contributed to improving the efficiency transformation between the PEO and the curcumin NPs. Our results are in good agreement with the similar report of a decrease in the optical gap energy from 4.6 eV to 2.7 eV with increasing

polyaniline content from 0.5 to 5 wt.% [24]. In the literature, a similar reduction was also found in the value of the absorption edge from 6.2 eV in the case of pure PEO to 2.9 eV in PEO with Ag NPs [25]. To compare the different thicknesses of PEO-Curcumin composites, the value of the energy band gap evaluated ($h\nu$) is 2.56 eV for the thin film of 250 nm thickness and 2.48 eV for both thin films of 500 and 750 nm. The results reveal that these comparable absorption coefficient values with no significant differences between curcumin and PEO-Curcumin and between 500 and 750 nm film thickness indicate that the absorption coefficient spectra had similar spectral variations Curcumin and PEO-Curcumin as well as 500 and 750 nm thickness.

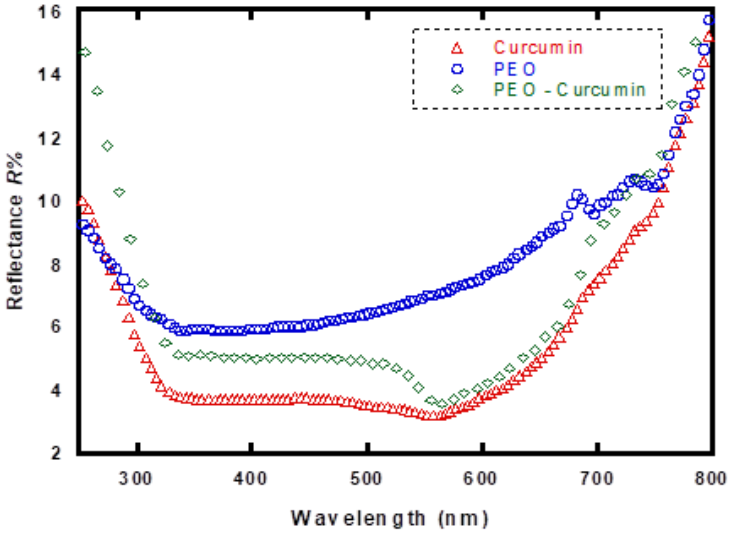

Figure 6. Reflectance spectra of PEO, curcumin, and PEO-Curcumin thin films with an average thickness of 500 nm.

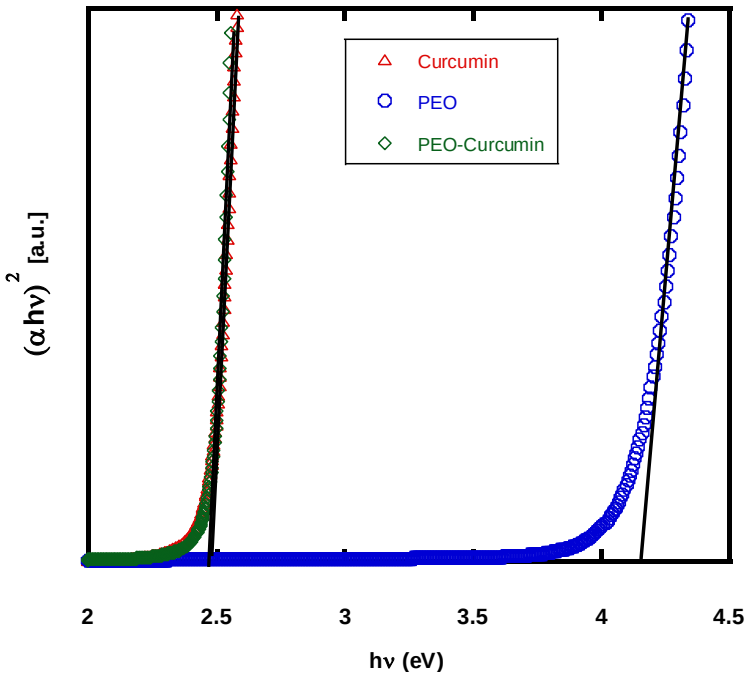

Figure 7. Tauc optical bandgap energy of pure PEO, curcumin NPs, PEO-Curcumin nanocomposite thin films.

Nanocomposite thin films with thicknesses 250, 500, and 700 nm were investigated to obtain the effect of film thickness on PEO-Curcumin nanocomposite's optical properties. The transmittance spectra for PEO-Curcumin nanocomposite thin films with thicknesses 250, 500, and 750 nm are shown in Fig. 8. It can be seen that PEO-Curcumin nanocomposites thin film

with a thickness of 250 nm exhibits high transmittance above 500 nm. The absorption region's edge was shifted into a red region with lower energy as film thickness increased to 750 nm. This can relate to the high electron transition from the valence band to the curcumin's conduction band. The transmittance values for PEO-Curcumin decreased when the film thickness increased to 750 nm with no significant changes between 500 and 750 nm. This decrease in transmittance, in turn, enhanced the absorption of light due to the increase of the film thickness. This is because of higher thickness; the films became more saturated with curcumin, decreasing transmittance.

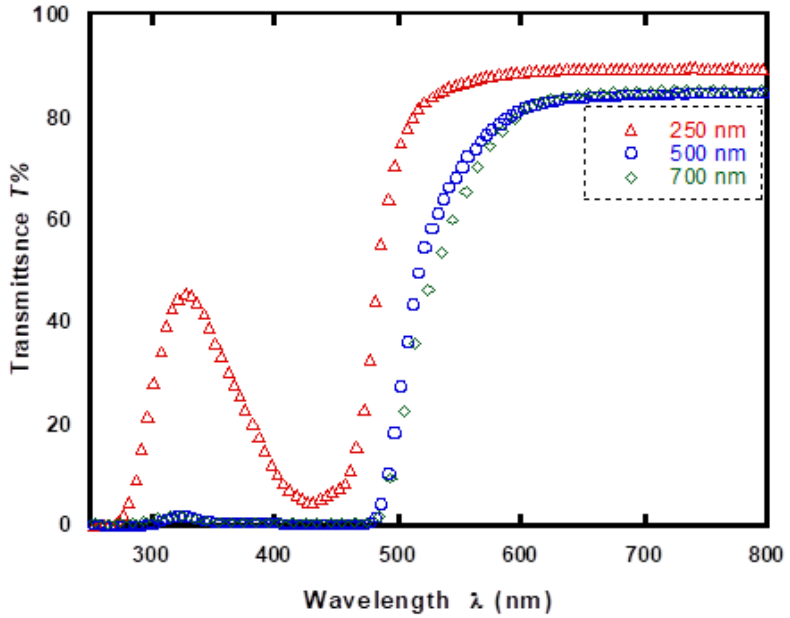

Figure 8. Transmittance spectra of PEO-Curcumin thin films with thicknesses 250, 500, and 750 nm.

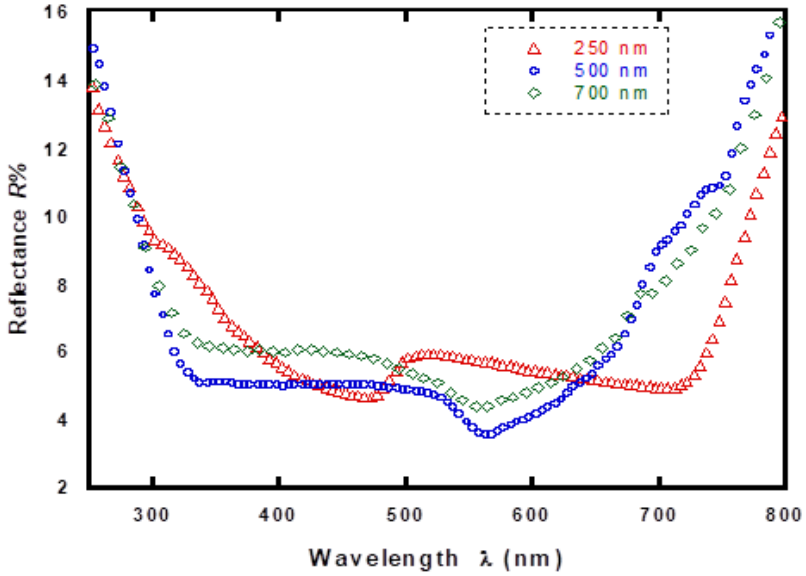

Figure 9. Reflectance spectra of PEO-Curcumin thin films with thicknesses 250, 500, and 750 nm.

Interestingly, the peak of lower film thickness around 330 nm in Figure 8 with a transmittance of about 50 % could be used as a bandpass filter for these regions. Figure 9 shows the reflectance spectra for PEO-Curcumin nanocomposites thin films with 250, 500, and 750 nm thicknesses. The reflectance for all samples has the same values on average due to the surface of these films having the exact nature for PEO-Curcumin nanocomposites thin films.

Fig. 10 is the film thickness-dependent Tauc plot for PEO-Curcumin thin films. The samples consist of a fixed concentration of PEO and variable concentrations of curcumin. The bandgap energy of PEO-Curcumin nanocomposites thin films with a thickness of 250 nm was found to be 2.56 eV, this value comparable to the values of 500 and 700 nm (2.48 eV). Bandgap energy decreases with increasing film thicknesses due to a higher concentration of curcumin NPs added to the PEO compound. No significant changes in the optical bandgap energy were noticed between 500 and 750 nm.

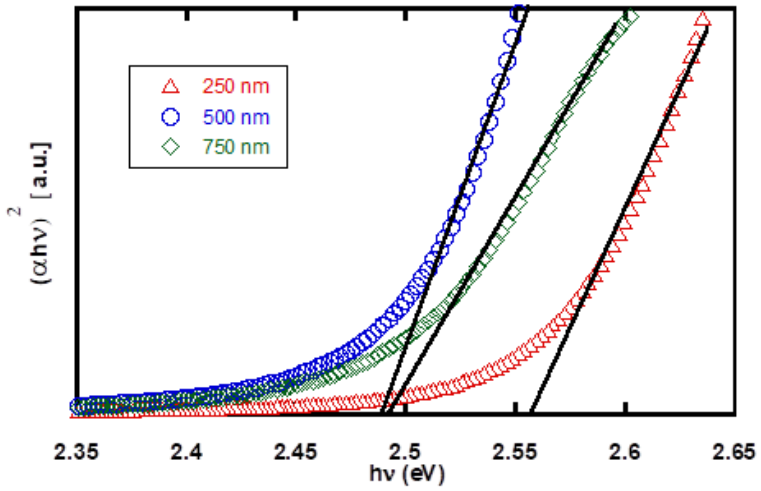

Figure 10. Tauc optical band gap energy of PEO-Curcumin thin films with film thickness 250, 500, and 750 nm.

The amount of light energy dissipated by absorption and scattering in the thin films is represented as the extinction coefficient. The extinction coefficient values are dependent on the density of free electrons and the structural distortion in the thin films. The curves of extinction coefficient, ε, are calculated from the equation $\boldsymbol{\varepsilon = \alpha\lambda/4\pi}$ [26,27] where: α is the optical absorption coefficient defined by $\alpha = (1/t)\mathrm{Ln}((1-R)^2/T)$, where t is the coated film thickness (500 nm), T, the transmittance of the light through the sample, and R is the reflectance of the light from the surface of the sample [28]. Thus, the study of optical absorption coefficient (α) spectra for nanocomposite thin films provides essential information about the optical band gap energy (E_g) and determines the material capacity for absorbing light [29–32]. Extinction coefficient (ε) values of PEO-Curcumin thin films with thicknesses 250, 500, and 750 nm are shown in Figure 11. The extinction coefficient values rapidly decrease after reaching the maximum value of ε and approaching zero in the wavelength of 550 nm and above. This indicates that these film materials allow electromagnetic photons to pass through the material without any damping or decay in the wavelength's visible region. For example, the extinction coefficient for PEO-Curcumin nanocomposite thin film at 250 nm has the highest value of ε = 0.42 around the wavelength 431 nm. This value decreased to 0.40 and 0.25 for the 500 and 750 nm thicknesses, respectively.

Furthermore, we noticed a significant shift in the maximum peak of the 250 nm film from 431 to around 473 nm for both thicknesses of 500 and 750 nm. This indicates that the samples have a higher amount of light energy loss by scattering and absorption. No significant changes in the ε values after 470 nm; the ε -values were changed slightly, which means that the absorption and scattering loss of energy per unit distance has small values when light propagates through nanocomposite thin films [33,34].

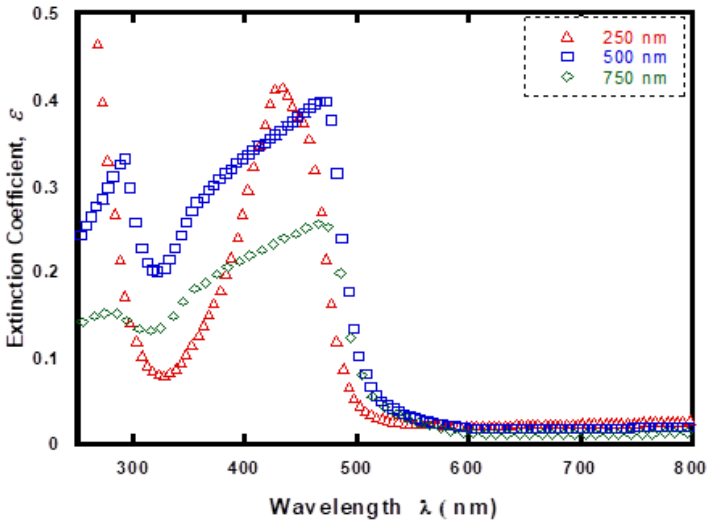

Figure 11. Extinction coefficient spectra of PEO-Curcumin thin films with thicknesses 250, 500, and 750 nm.

The absorption coefficient is one of the inherent optical properties determined by transmittance and reflectance measurements. Knowledge of the optical absorption coefficient is another approach to understanding the bandgap energy of nanocomposite films. Figure 12 represents the typical optical absorption coefficient (α) versus the wavelength for nanocomposite films of PEO, curcumin, and PEO-Curcumin with 500 nm thickness. The light propagation through the three sets of samples slab each of 500 nm thickness, depends not merely on the thickness but also the composite concentration. The absorption coefficient is usually measured to represent the probability per infinitesimal path length photons absorbs. We have found that the optical absorption coefficients in Figure 12 are independent of wavelength greater than 500 nm and strongly dependent below this wavelength. The absorption coefficient is calculated for the three sets of the samples at the thickness of 250, 500, and 750 nm, respectively. As shown in Figure 13, it is evident that the optical absorption coefficient is strongly dependent on the film thickness and increases with decreasing the film thicknesses [35]. The absorption coefficient at a wavelength greater than 500 nm slightly increases at the thickness of 250 nm and remains constant at 500 and 750 nm.

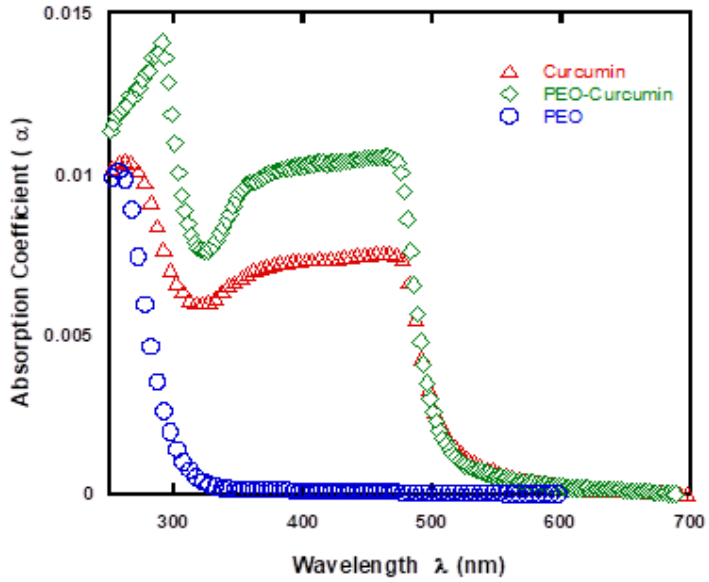

Figure 12. Optical absorption coefficient (α) spectra of nanocomposite films with a thickness 500 nm were obtained for PEO, curcumin, and PEO-Curcumin nanocomposite.

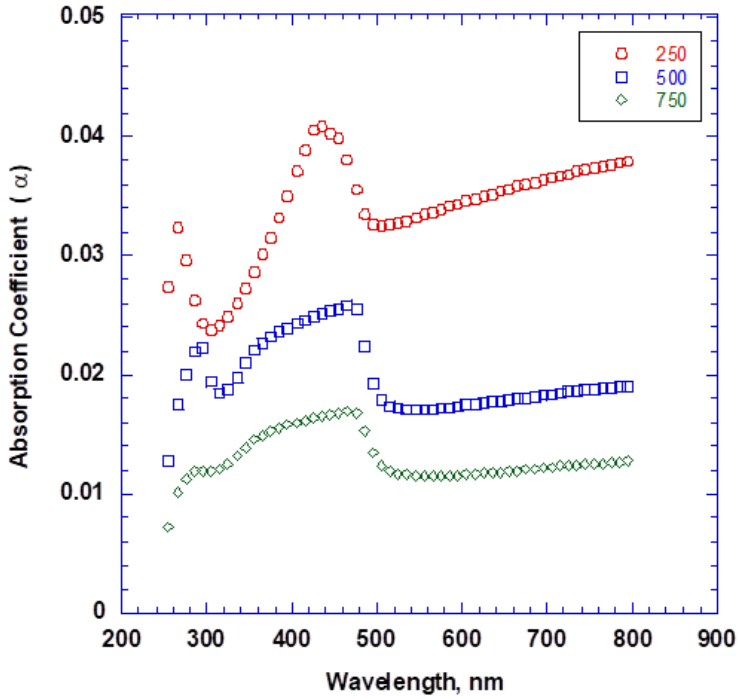

Figure 13. Optical absorption coefficient (α) spectra for nanocomposite films of PEO-Curcumin with thicknesses 250, 500, and 750 nm.

The study of refractive index behavior is essential in many optical phenomena. The Refractive index, n, is closely related to ions' electronic polarization and the local field inside the optical materials[39]. The refractive index curves, n, shown in Figure 14, are calculated from the equation $\boldsymbol{n} = (\frac{\mathbf{1+R}}{\mathbf{1-R}}) + \sqrt{(\mathbf{4R/(1-R)^2}) - \boldsymbol{\varepsilon}^{\mathbf{2}}}$ [26,36,37].The refractive index (n) curves are for PEO-Curcumin thin films with thicknesses 250, 500, and 750 nm as a function of incident light wavelength.

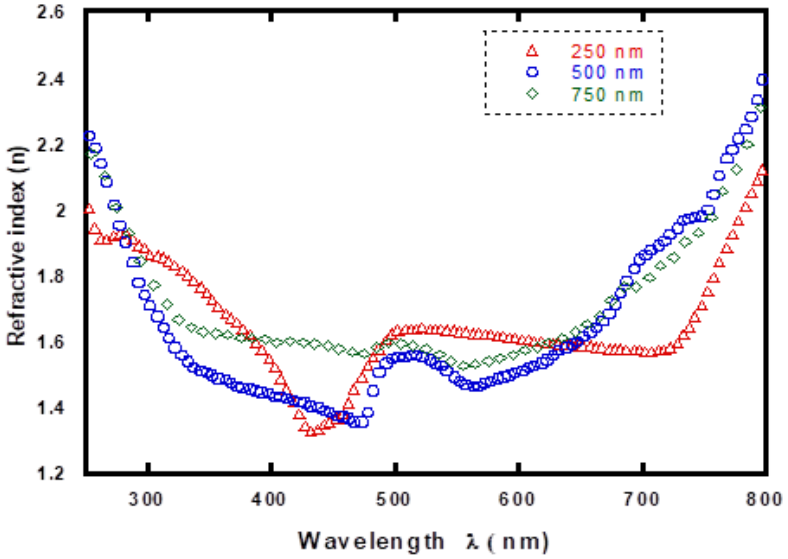

Figure 14. Refractive index spectra of PEO-Curcumin thin films with thicknesses 250, 500, and 750 nm.

From Fig.14, it is observed that the refractive index is divided into two regions; at λ<350 nm, which represents anomalous behavior, and at λ>350 nm, which represents a normal dispersion. Furthermore, it was also seen that in the vital absorption region (λ<350 nm), the incident photon frequency becomes almost equal to the plasma frequency and owing to the

refractive index of higher values in this region [38]. Therefore, a resonance effect will arise between the incident EM photons and the electron polarization. This led to the coupling of electrons in nanocomposite thin films to the oscillating electric field. By that, EM radiation propagation through thin films will be constricted, but it may prevent these EM waves' propagation [39]. The refractive index sharply decreases in the visible region as the wavelength increases and shows significant normal dispersion. The Refractive index for all thin films exhibits the same values ranging between 1.5 and 2.0.

4. Conclusions

PEO-Curcumin thin films were prepared by a simple spin-coating technique. The films obtained were characterized using SEM, FTIR, and UV-reflectance spectroscopy. The curcumin nanoparticles are spherical with an average size of less than 100 nm, with a significant agglomeration of nanoparticles upon forming the composite membrane. The particles' size distribution should have been originated from the large specific surface area and high surface energy of curcumin NPs. FTIR vibrational bands observed at 1023 and 1120 cm^{-1} are attributed to stretching of C–O stretching vibration; a band at 1453 cm^{-1} could be ascribed to the $–CH_2$ bending vibration, while bands appearing in 2950–2700 could be ascribed to the symmetric and asymmetric C–H stretching modes of the CH_2 group. At the same time, PEO-Curcumin nanoparticle thin films have additional peaks which correspond to curcumin structure. The vibrational band at 804 cm^{-1} is assigned to bending C–H, a band at 1237 and 1280 cm^{-1} is attributed to the C–O bending vibration, and a band appearing at 1340 cm^{-1} could be ascribed to O-H bending. Thus, there are significant changes observed in width and the intensity of the vibrational bands of PEO upon formation of PEO-Curcumin thin films.

The transmittance spectra for PEO, Curcumin, and PEO-Curcumin thin films with an average thickness of 500 nm are obtained. PEO thin film exhibits high transmittance above 300 nm, while curcumin thin film exhibits high transparent above 600 nm. This confirms that the bandgap energy for curcumin is less than PEO. PEO-Curcumin thin film has high transmittance above 600 nm; the edge of the absorption region is found to be shifted into the red region for the curcumin NPs in PEO film. This leads to high electron transition through the energy bandgap performed by transition electrons between the valence and conduction bands for curcumin. The reflectance of the thin films decreases with the increase in curcumin NPs concentration. Refraction index (n) had values between 1.5 and 2 for PEO-Curcumin, which increases with an increase in thicknesses. Optical bandgap energy of PEO thin film was found to be 4.16 eV, while Curcumin NPs and PEO-Curcumin NPs thin films have less bandgap energy of 2.49 eV, optical band gap energy decreases with increasing film thicknesses.

Funding

The authors would like to thank Jordan University of Science and Technology in Jordan for the Deanship of Scientific Research's support with grant number 481/2081.

Acknowledgments

Special thanks to Leibniz-Institut für Analytische Wissenschaften-ISAS Germany for the best collaboration that has been done with Jordan University of Science and Technology.

Conflicts of Interest

The authors declare no conflict of interest.

References

1. Mantzorou, M.; Pavlidou, E.; Vasios, G.; Tsagalioti, E.; Giaginis, C. Effects of Curcumin Consumption on Human Chronic Diseases: A Narrative Review of the Most Recent Clinical Data. *Phytotherapy Research* **2018**, *32*, 957–975, https://doi.org/10.1002/ptr.6037.
2. Narayanaswamy, V.; Alaabed, S.; Issa, B.; AL-Akhras, M.-A.; Obaidat, I.M. Molecular Simulation of Curcumin Loading on Graphene and Graphene Oxide for Drug Delivery Applications. *Current Chemistry Letters* **2021**, *10*, 161–168, https://doi.org/10.5267/j.ccl.2020.12.003.
3. Semlali, A.; Contant, C.; Al-Otaibi, B.; Al-Jammaz, I.; Chandad, F. The Curcumin Analog (PAC) Suppressed Cell Survival and Induced Apoptosis and Autophagy in Oral Cancer Cells. *Sci Rep* **2021**, *11*, https://doi.org/10.1038/s41598-021-90754-x.
4. Marton, L.T.; Pescinini-e-Salzedas, L.M.; Camargo, M.E.C.; Barbalho, S.M.; Haber, J.F.S.; Sinatora, R.V.; Detregiachi, C.R.P.; Girio, R.J.S.; Buchaim, D.V.; Cincotto dos Santos Bueno, P. The Effects of Curcumin on Diabetes Mellitus: A Systematic Review. *Frontiers in Endocrinology* **2021**, *12*, https://doi.org/10.3389/fendo.2021.669448.
5. Sharifi-Rad, J.; Rayess, Y.E.; Rizk, A.A.; Sadaka, C.; Zgheib, R.; Zam, W.; Sestito, S.; Rapposelli, S.; Neffe-Skocińska, K.; Zielińska, D.; Salehi, B.; Setzer, W.N.; Dosoky, N.S.; Taheri, Y.; El Beyrouthy, M.; Martorell, M.; Ostrander, E.A.; Suleria, H.A.R.; Cho, W.C.; Maroyi, A.; Martins, N. Turmeric and Its Major Compound Curcumin on Health: Bioactive Effects and Safety Profiles for Food, Pharmaceutical, Biotechnological and Medicinal Applications. *Front Pharmacol* **2020**, *11*, https://doi.org/10.3389/fphar.2020.01021.
6. Manolova, Y.; Deneva, V.; Antonov, L.; Drakalska, E.; Momekova, D.; Lambov, N. The Effect of the Water on the Curcumin Tautomerism: A Quantitative Approach. *Spectrochimica Acta Part A: Molecular and Biomolecular Spectroscopy* **2014**, *132*, 815–820, https://doi.org/10.1016/j.saa.2014.05.096.
7. Sinha, D.; De, D.; Ayaz, A. Performance and Stability Analysis of Curcumin Dye as a Photo Sensitizer Used in Nanostructured ZnO Based DSSC. *Spectrochimica acta. Part A, Molecular and biomolecular spectroscopy* **2018**, *193*, 467-474, https://doi.org/10.1016/j.saa.2017.12.058.
8. Kumari, M.; Sharma, N.; Manchanda, R.; Gupta, N.; Syed, A.; Bahkali, A.H.; Nimesh, S. PGMD/Curcumin Nanoparticles for the Treatment of Breast Cancer. *Sci Rep* **2021**, *11*, https://doi.org/10.1038/s41598-021-81701-x.
9. Salarbashi, D.; Tafaghodi, M.; Fathi, M.; Aboutorabzade, S.M.; Sabbagh, F. Development of Curcumin-Loaded Prunus Armeniaca Gum Nanoparticles: Synthesis, Characterization, Control Release Behavior, and Evaluation of Anticancer and Antimicrobial Properties. *Food Science & Nutrition* **2021**, *9*, 6109–6119, https://doi.org/10.1002/fsn3.2562.
10. Trigo-Gutierrez, J.K.; Vega-Chacón, Y.; Soares, A.B.; Mima, E.G.O. Antimicrobial Activity of Curcumin in Nanoformulations: A Comprehensive Review. *International Journal of Molecular Sciences* **2021**, *22*, https://doi.org/10.3390/ijms22137130.
11. Abdulwahab, F.; Henari, F.Z.; Cassidy, S.; Winser, K. Synthesis of Au, Ag, Curcumin Au/Ag, and Au-Ag Nanoparticles and Their Nonlinear Refractive Index Properties. *Journal of Nanomaterials* **2016**, *2016*, https://doi.org/10.1155/2016/5356404.
12. Tabanelli, R.; Brogi, S.; Calderone, V. Improving Curcumin Bioavailability: Current Strategies and Future Perspectives. *Pharmaceutics* **2021**, *13*, https://doi.org/10.3390/pharmaceutics13101715.
13. Nelson, K.M.; Dahlin, J.L.; Bisson, J.; Graham, J.; Pauli, G.F.; Walters, M.A. The Essential Medicinal Chemistry of Curcumin. *J. Med. Chem.* **2017**, *60*, 1620–1637, https://doi.org/10.1021/acs.jmedchem.6b00975.
14. AL-Akhras, M.-A.; Alzoubi, S.E.; Ahmad, A.A.; Ababneh, R.; Telfah, A. Studies of Composite Films of Polyethylene Oxide Doped with Potassium Hexachloroplatinate. *Journal of Applied Polymer Science* **2021**, *138*, https://doi.org/10.1002/app.49757.
15. Telfah, A.; Al-Akhras, M.; Al-izzy, K.A.; Ahmad, A.A.; Ababneh, R.; Ahmad, M.J.A.; Tavares, C.; Hergenröder, R. Dielectric Relaxation, XPS and Structural Studies of Polyethylene Oxide/Iodine Complex Composite Films. *Polymer Bulletin* **2021**, https://doi.org/10.1007/s00289-021-03593-1.
16. Kianfar, P.; Vitale, A.; Dalle Vacche, S.; Bongiovanni, R. Enhancing Properties and Water Resistance of PEO-Based Electrospun Nanofibrous Membranes by Photo-Crosslinking. *J Mater Sci* **2021**, *56*, 1879–1896, https://doi.org/10.1007/s10853-020-05346-3.
17. Mbaya, A.; Kumshe, H.; Alaka, O.; Kyari, F. Effect of Polyethylene Glycol on Single and Combined Topical Application of Diminazene Aceturate (Berenil) and Metronidazole (Metrodine) in Trypanosoma Brucei- and T. Congolense-Infected Mice. *Comparative Clinical Pathology* **2014**, *23*, https://doi.org/10.1007/s00580-012-1632-1.

18. Mohan, V.M.; Raja, V.; Sharma, A.K.; Rao, V.V.R.N. Ion Transport and Battery Discharge Characteristics of Polymer Electrolyte Based on PEO Complexed with $NaFeF_4$ Salt. *Ionics* **2006**, *3*, 219–226, https://doi.org/10.1007/s11581-006-0035-1.
19. Papke, B.L.; Ratner, M.A.; Shriver, D.F. Vibrational Spectroscopic Determination of Structure and Ion Pairing in Complexes of Poly(Ethylene Oxide) with Lithium Salts. *J. Electrochem. Soc.* **1982**, *129*, 1434, https://doi.org/10.1149/1.2124179.
20. Konuk Ege, G.; Yüce, H.; Akay, Ö.; Öner, H.; Genç, G. A Fabrication and Characterization of Luffa/PANI/PEO Biocomposite Nanofibers by Means of Electrospinning. *Pigment & Resin Technology* **2021**, https://doi.org/10.1108/PRT-09-2021-0105.
21. Tauc, J. *Amorphous and Liquid Semiconductors*. Springer Science & Business Media, **2012.**
22. Essahlaoui, A.; Essaoudi, H.; Hallaoui, A.; Mohamed, B.; Labzour, A.; Housni, A. Calculation of the Thickness and Optical Constants of Lead Titanate Thin Films Grown on MgO from Their Transmission Spectra. *Journal of Materials and Environmental Science* **2018**, *9*, 228–234, https://doi.org/10.26872/jmes.2018.9.1.26.
23. Bhattacharyya, D.; Chaudhuri, S.; Pal, A. Bandgap and Optical Transitions in Thin Films from Reflectance Measurements. *Vacuum* **1992**, *43*, 313–316, https://doi.org/10.1016/0042-207X(92)90163-Q.
24. Mezdour, D.; Bardeau, J.-F.; Errien, N.; Pilard, J.-F.; Tabellout, M. Polyaniline Based Composite Layers for Photovoltaïc Applications: Thermal and Optical Properties Investigation. *AIP Conference Proceedings* **2019**, *2196*, https://doi.org/10.1063/1.5140275.
25. Aziz, S.B.; Marif, R.B.; Brza, M.; Hassan, A.N.; Ahmad, H.A.; Faidhalla, Y.A.; Kadir, M. Structural, Thermal, Morphological and Optical Properties of PEO Filled with Biosynthesized Ag Nanoparticles: New Insights to Band Gap Study. *Results in Physics* **2019**, *13*, https://doi.org/10.1016/J.RINP.2019.102220.
26. Ahmad, A.; Alsaad, A.; Al-Bataineh, Q.; Al-Naafa, M. Optical and Structural Investigations of Dip-Synthesized Boron-Doped ZnO-Seeded Platforms for ZnO Nanostructures. *Applied Physics A* **2018**, *124*, https://doi.org/10.1007/s00339-018-1875-z.
27. Al-Bataineh, Q.; Alsaad, A.; Ahmad, A.; Al-Sawalmih, A. Structural, Electronic and Optical Characterization of ZnO Thin Film-Seeded Platforms for ZnO Nanostructures: Sol–Gel Method Versus Ab Initio Calculations. *Journal of Electronic Materials* **2019**, *48*, https://doi.org/10.1007/s11664-019-07303-6.
28. Al-Bataineh, Q.M.; Telfah, M.; Ahmad, A.A.; Alsaad, A.M.; Qattan, I.A.; Baaziz, H.; Charifi, Z.; Telfah, A. Synthesis, Crystallography, Microstructure, Crystal Defects, Optical and Optoelectronic Properties of $ZnO:CeO_2$ Mixed Oxide Thin Films. *Photonics* **2020**, *7*, https://doi.org/10.3390/photonics7040112.
29. Khan, S.; Al-Hazmi, F.; Heniti, S.; Faidah, A.; Al-Ghamdi, A. Effect of Cadmium Addition on the Optical Constants of Thermally Evaporated Amorphous Se–S–Cd Thin Films. *Current Applied Physics* **2010**, *10*, 145–152, https://doi.org/10.1016/j.cap.2009.05.010.
30. Urbach, F. The Long-Wavelength Edge of Photographic Sensitivity and of the Electronic Absorption of Solids. *Phys. Rev.* **1953**, *92*, 1324–1324, https://doi.org/10.1103/PhysRev.92.1324.
31. El-Hagary, M.; Emam-Ismail, M.; Shaaban, E.; El-Taher, A. Effect of γ-Irradiation Exposure on Optical Properties of Chalcogenide Glasses Se70S30−xSbx Thin Films. *Radiation Physics and Chemistry* **2012**, *81*, 1572–1577, https://doi.org/10.1016/j.radphyschem.2012.05.012.
32. Ahmad, A.A.; Alsaad, A.M.; Al-Bataineh, Q.M.; Al-Akhras, M.-A.H.; Albataineh, Z.; Alizzy, K.A.; Daoud, N.S. Synthesis and Characterization of ZnO NPs-Doped PMMA-BDK-MR Polymer-Coated Thin Films with UV Curing for Optical Data Storage Applications. *Polym. Bull.* **2021**, *78*, 1189–1211, https://doi.org/10.1007/s00289-020-03155-x.
33. Davis, E.A.; Mott, N.F. Conduction in Non-Crystalline Systems V. Conductivity, Optical Absorption and Photoconductivity in Amorphous Semiconductors. *The Philosophical Magazine: A Journal of Theoretical Experimental and Applied Physics* **1970**, *22*, 0903–0922, https://doi.org/10.1080/14786437008221061.
34. Mott, N.F.; Davis, E.A. *Electronic Processes in Non-Crystalline Materials*. Oxford Classic Texts in the Physical Sciences; Oxford University Press: Oxford, New York, **2012**.
35. Tashtoush, N.; Sheiab, A.; Jafar, M.; Momani, S. Determining Optical Constants of Sol-Gel Vanadium Pentoxide Thin Films Using Transmittance and Reflectance Spectra. *International Journal of Physics: Study and Research* **2019**, *2*, 59–64, https://doi.org/10.18689/ijpsr-1000108.
36. Al-Bataineh, Q.; Ahmad, A.; Alsaad, A.; Salameh, A. Optical and Structural Characterization of Dip Synthesized Al-B Co-Doped ZnO Seeded Platforms for ZnO Nanostructures. *Materials Science* **2018**.
37. Ahmad, A.A.; Alsaad, A.M.; Albiss, B.A.; Al-Akhras, M.-A.; El-Nasser, H.M.; Qattan, I.A. Optical and Structural Properties of Sputter Deposited ZnO Thin Films in Relevance to Post-Annealing and Substrate Temperatures. *Thin Solid Films* **2016**, *C*, 133–142, https://doi.org/10.1016/j.tsf.2016.03.041.
38. Hassanien, A.S.; Sharma, I. Optical properties of quaternary a-Ge15-x Sbx Se50 Te35 thermally evaporated thin-films: refractive index dispersion and single oscillator parameters. *Optik* **2020**, *200*, https://doi.org/10.1016/j.ijleo.2019.163415.
39. Hassanien, A.S. Studies on Dielectric Properties, Opto-Electrical Parameters and Electronic Polarizability of Thermally Evaporated Amorphous $Cd_{50}S_{50-x}Se_x$ Thin Films. *Journal of Alloys and Compounds* **2016**, *671*, 566–578, https://doi.org/10.1016/j.jallcom.2016.02.126.